**Supporting Information**

# Variable-temperature ESI-IMS-MS analysis of myohemerythrin reveals ligand losses, unfolding, and a non-native disulfide bond

Daniel W. Woodall, [1] Tarick J. El-Baba, [1] Daniel R. Fuller, [1] Wen Liu,[2] Christopher J. Brown,[1] Arthur Laganowsky,[2] David H. Russell,[2] and David E. Clemmer[1,*]

[1] Department of Chemistry, Indiana University, Bloomington, Indiana, 47405

[2] Department of Chemistry, Texas A&M University, College Station, Texas, 77843

*Corresponding author:
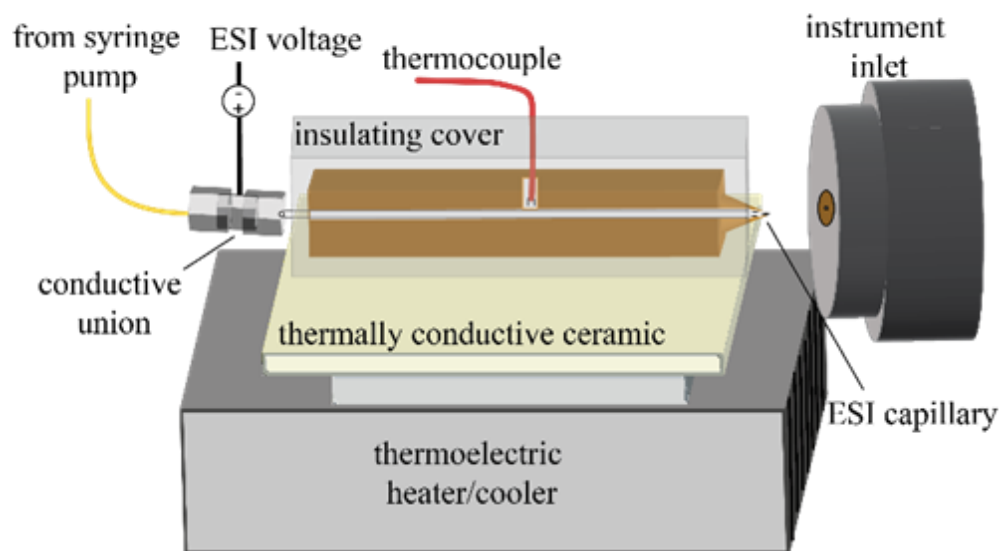
David E. Clemmer

clemmer@indiana.edu

**Figure S1.** Schematic diagram of vT-ESI device for controlling solution temperature of protein solution.

**Table S1.** *m/z* values of observed Mhr species

| charge state | hMhr-O2 [a] 14081.5 Da | hMhr [b] 14049.5 Da | aMhr [c] 13921.9 Da | aMhr-ox [d] 13937.9 Da | aMhr-2ox [e] 13953.8 Da |
|:---:|:---:|:---:|:---:|:---:|:---:|
| 5 | - | 2810.01 | 2785.05 | - | - |
| 6 | 2348.03 | 2341.88 | 2321.09 | 2323.91 | 2326.94 |
| 7 | 2012.71 | 2007.33 | 1989.77 | 1992.05 | 1994.34 |
| 8 | 1761.26 | 1756.48 | 1471.04 | 1743.12 | 1745.03 |
| 9 | - | 1566.44 | 1547.79 | 1549.45 | 1551.26 |
| 10 | - | - | 1393.11 | 1394.61 | 1396.3 |
| 11 | - | - | 1266.46 | 1267.82 | 1269.56 |
| 12 | - | - | 1161.08 | 1162.32 | 1163.74 |
| 13 | - | - | 1071.77 | 1072.92 | -* |
| 14 | - | - | 995.28 | 996.48 | 997.7 |
| 15 | - | - | 928.91 | 930.12 | 931.25 |
| 16 | - | - | 870.98 | 871.98 | - |

[a] $O_2$ bound holomyohemerythrin species

[b] Holomyohemerythrin species

[c] Apomyohemeryhtrin species

[d] Apomyohemerythrin with single oxidation modification

[e] Apomyohemerythrin with two oxidation modifications

* species not included in analysis due to the presence of an isobaric mass contaminant

Determination of metal cofactor charge: Supplemental figure S2 shows the high-resolution mass spectrum for the 7+ charge state of myohemerythrin (Mhr) under "native-like" conditions (30 mM aqueous ammonium acetate solution at room temperature). Charge deconvolution of the mass spectrum results in a mass ~4 Da lower than the expected mass for the holoprotein (14048.6 Da) because the deconvolution algorithm assumes that all charges are from the addition of protons. This difference indicates that the metal center has a net charge of 4+ for this species. This is consistent with the depiction of the active site in which the two Fe(III) metal atoms are coordinated by five neutral histidines, and two negatively charged carboxylate ligands from Asp111 and Glu58, to give a net charge of 4+. In the hMhr-$O_2$ species, the $O_2$ is formally bound as a negatively charged hydroperoxo (-OOH) ligand, which leads to a net charge of 3+ on the metal, and an addition of ~33 Da in the deconvoluted mass spectrum (Figure S2).
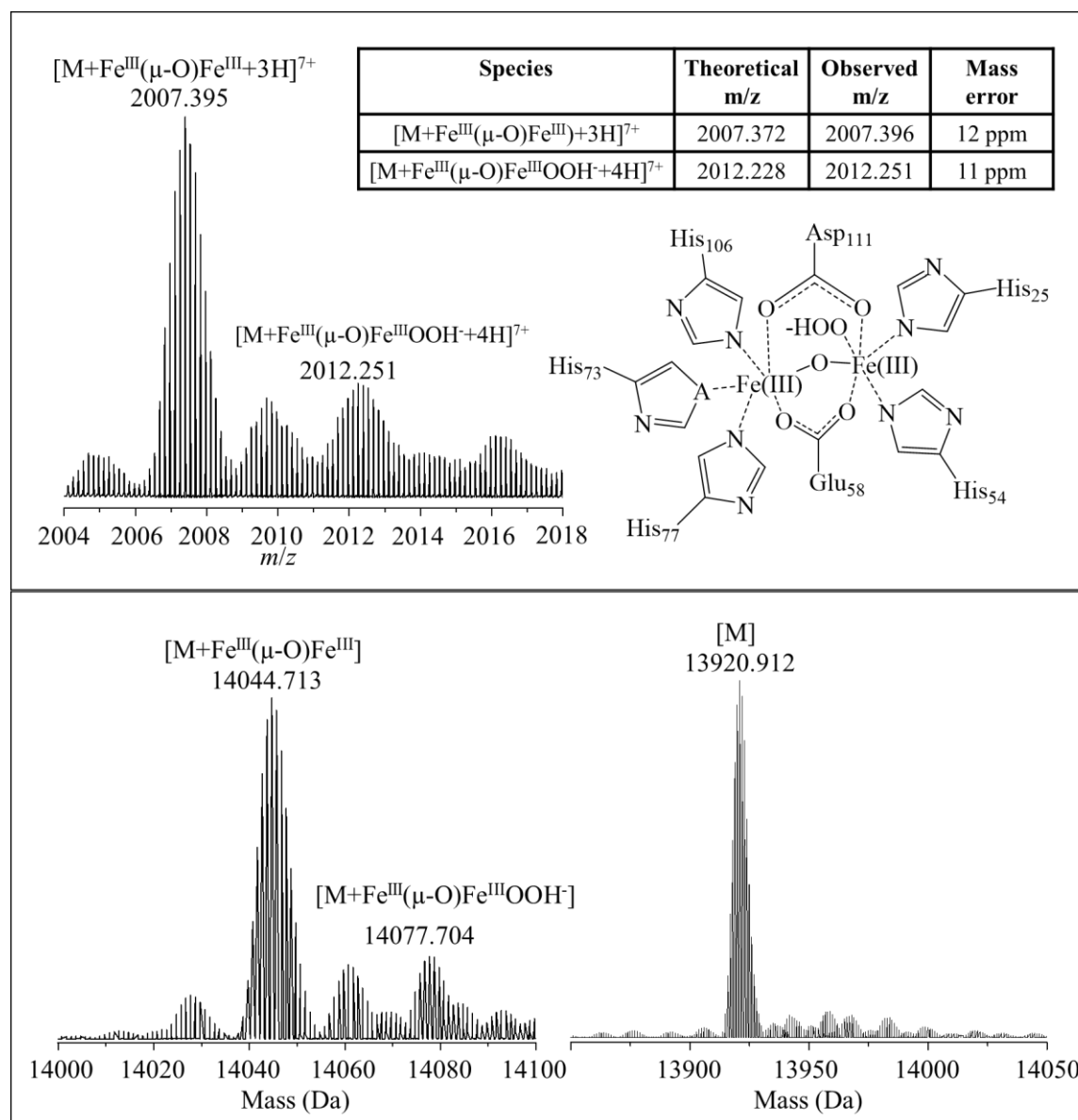
| Species | Theoretical m/z | Observed m/z | Mass error |
|---|---|---|---|
| $[M+Fe^{III}(\mu\text{-}O)Fe^{III})+3H]^{7+}$ | 2007.372 | 2007.396 | 12 ppm |
| $[M+Fe^{III}(\mu\text{-}O)Fe^{III}OOH^-+4H]^{7+}$ | 2012.228 | 2012.251 | 11 ppm |

**Figure S2.** High-resolution mass spectrum of the +7 charge state of holo-Mhr (top left) used in assignment of the ligation state and charge on the metal cofactor. Inset table displays theoretical $m/z$ values and oberseved values with reported mass error in these measurements. Active site coordinating residues are also shown in complex with the cofactor. Deconvoluted mass spectrum showing calculated mass for the holoprotein and $O_2$ bound species (bottom left) and the apoprotein (bottom right).

Assignment of IMS-MS features to conformer types according melting behavior. Supplemental figure S3 shows the abundance profiles of hMhr-$O_2$, hMhr, and aMhr that have been grouped together based on similarities in melting behavior. In the case of hMhr-$O_2$ the +6, +7, and +8 species each have two discernable features in their CCS distributions. In each charge state, the more compact feature has a midpoint $T_m = 66.0$ °C, and the more elongated feature at $T_m = \sim 64.0$ °C. Due to the similarities in melting behavior, and first derivative plots these six mobility features are grouped together into two distinct "native" conformer types designated N1 and N2. We then apply this analysis to the hMhr and aMhr species. We observe six distinguishable features in the mobility distributions of all the hMhr charge states, which we parse into three unique "native-like" conformer types.
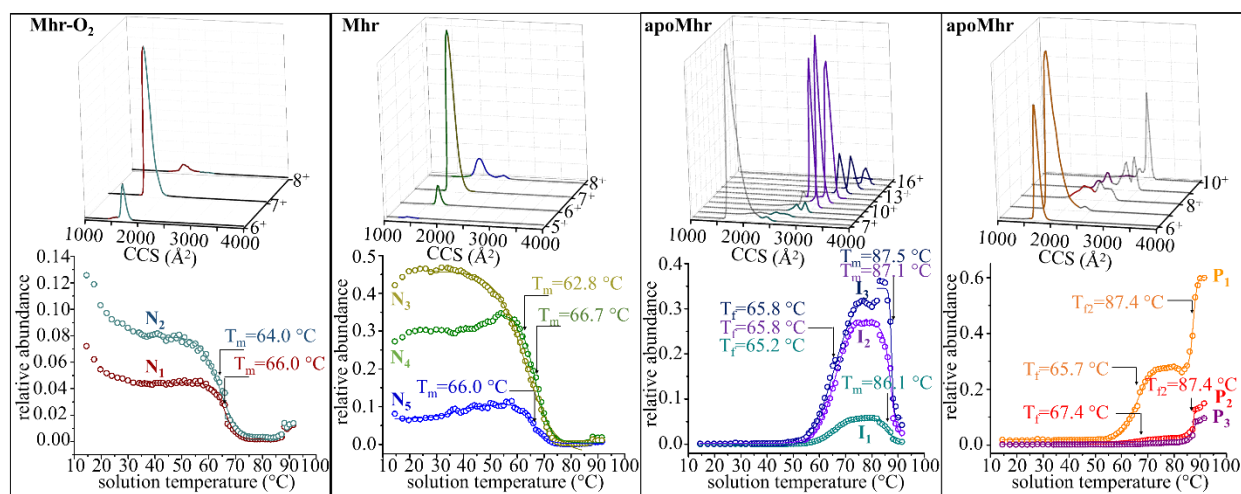


**Figure S3.** CCS distributions (top) and relative abundance plots (bottom) for the most abundant conformer types. IMS peaks with indistinguishable melting profiles are grouped and their summed abundances plotted as function of temperature to determine $T_m$. Colored regions of the CCS traces indicate IMS peak grouping bounds used to construct the abundance plots. Native (N) Mhr$_{(O2)}$ and hMhr states (N1 – N5) are shown in the left two panels, extended aMhr states I1 – I3 in the middle panel, and compact aMhr product states P1 – P3 in the right panel.

Loss of the metal cofactor at elevated temperature results in the formation of both highly-charged unfolded aMhr conformers, as well as compact aMhr with a more "native-like" charge

distribution and CCS. The extended aMhr species emerges as the hMhr species become unstable between ~55 to 75 °C. Interestingly, the extended apo states only persist over a narrow temperature range (~70 to 80 °C) upon which they undergo a second melting transition, resulting in a decrease in their abundance and a rise in the lower charged, compact aMhr states. Based on the curve shapes, and secondary melting temperatures, we identify five groups of high-temperature equilibrium intermediate states present in the extended conformations of charge states +5 to +16 of aMhr.  The three most abundant equilibrium intermediates are designated as I1, I2, I3 (Figure 6) and two low-abundant intermediate states are designated as I4 and I5  These conformer groups share similar formation temperatures ($T_f \approx 65$ °C), but are differentiated according to their unique melting behavior in the relatively narrow range of temperatures where they are stable (~70 to 80 °C). The population of compact aMhr conformers which appear to form concurrently with the extended aMhr species have similar midpoint formation temperature values of ~66 °C. At temperatures above 75 °C however, these compact conformer types remain stable and are classified as the stable products of melting. Analysis of their temperature profiles identifies three major products P1, P2, and P3, as well as three additional low abundance products P4 – P6. Product P1 is nearly indistinguishable from the extended I4 –I6 aMhr states in terms of $T_m$, however at ~80 °C (near the temperature at which conformers I1 and I2 begin to decay), P1 has a second growth phase with $T_{f\,=}$ 87.4 °C. Products P2 and P3 show similar behavior, only with lower relative abundance and slightly higher initial $T_f$ values.
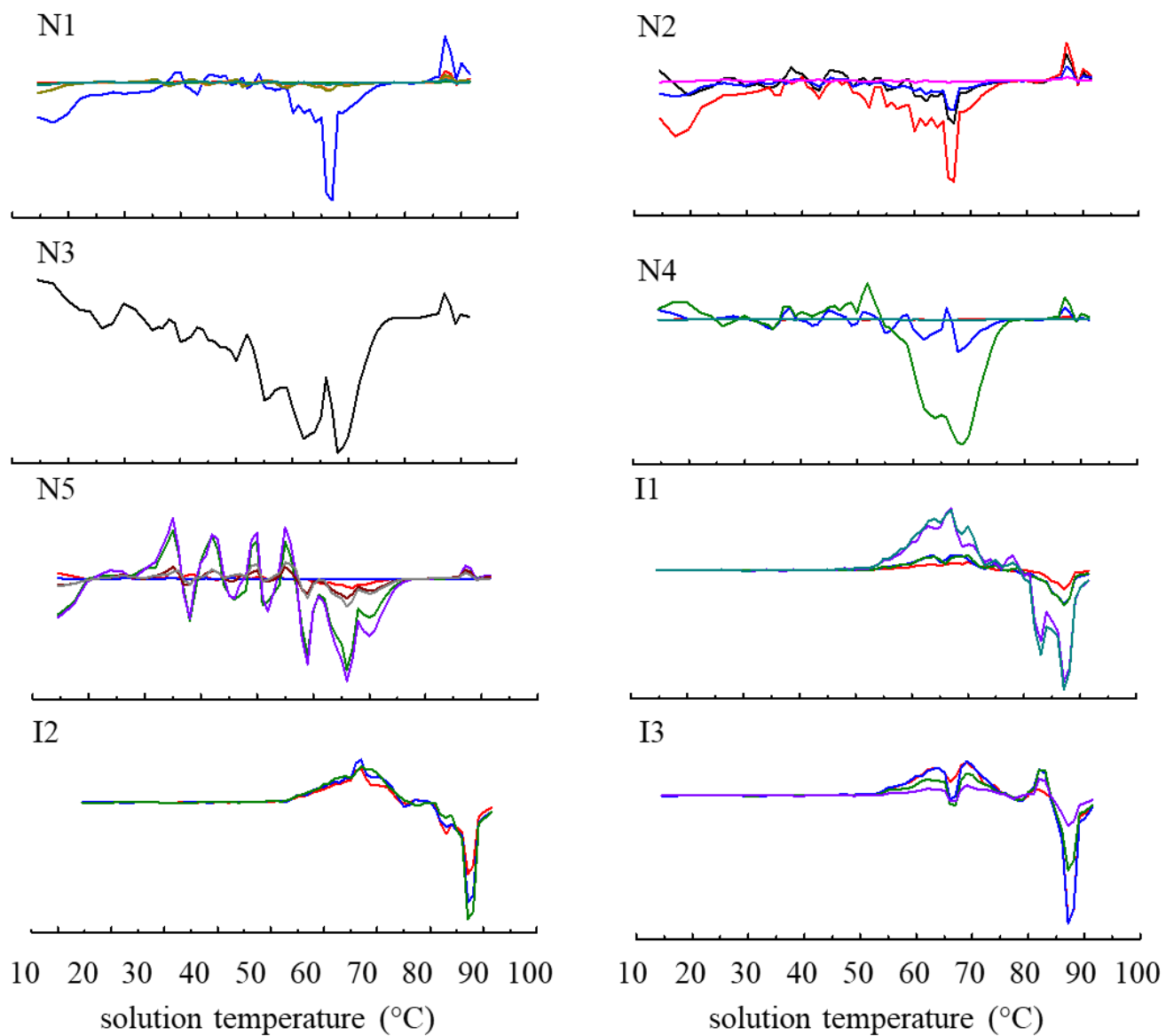
**Figure S4.** First derivative test plots used for grouping conformer types to identify those with similar melting behavior.
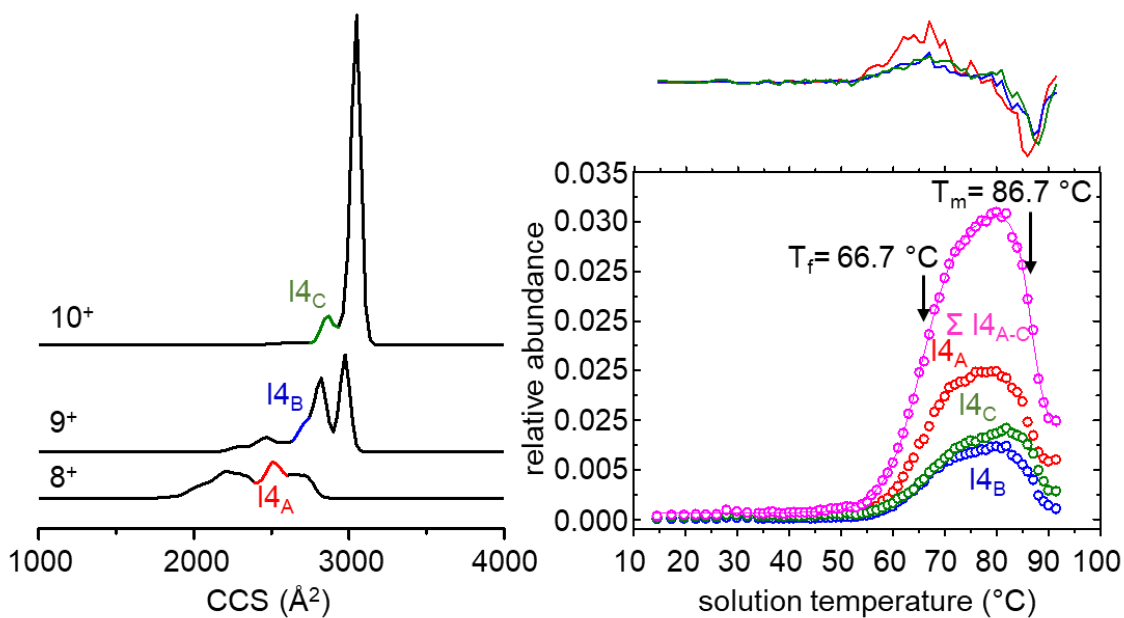
**Figure S5.** CCS distributions of low abundance intermediate conformer I4 (left), and abundance of the constituent IMS-MS features as a function of temperature (right). Colored regions in the CCS traces indicate integral bounds used in abundance plots. First derivative plots of each species are overlaid above the abundance plot.
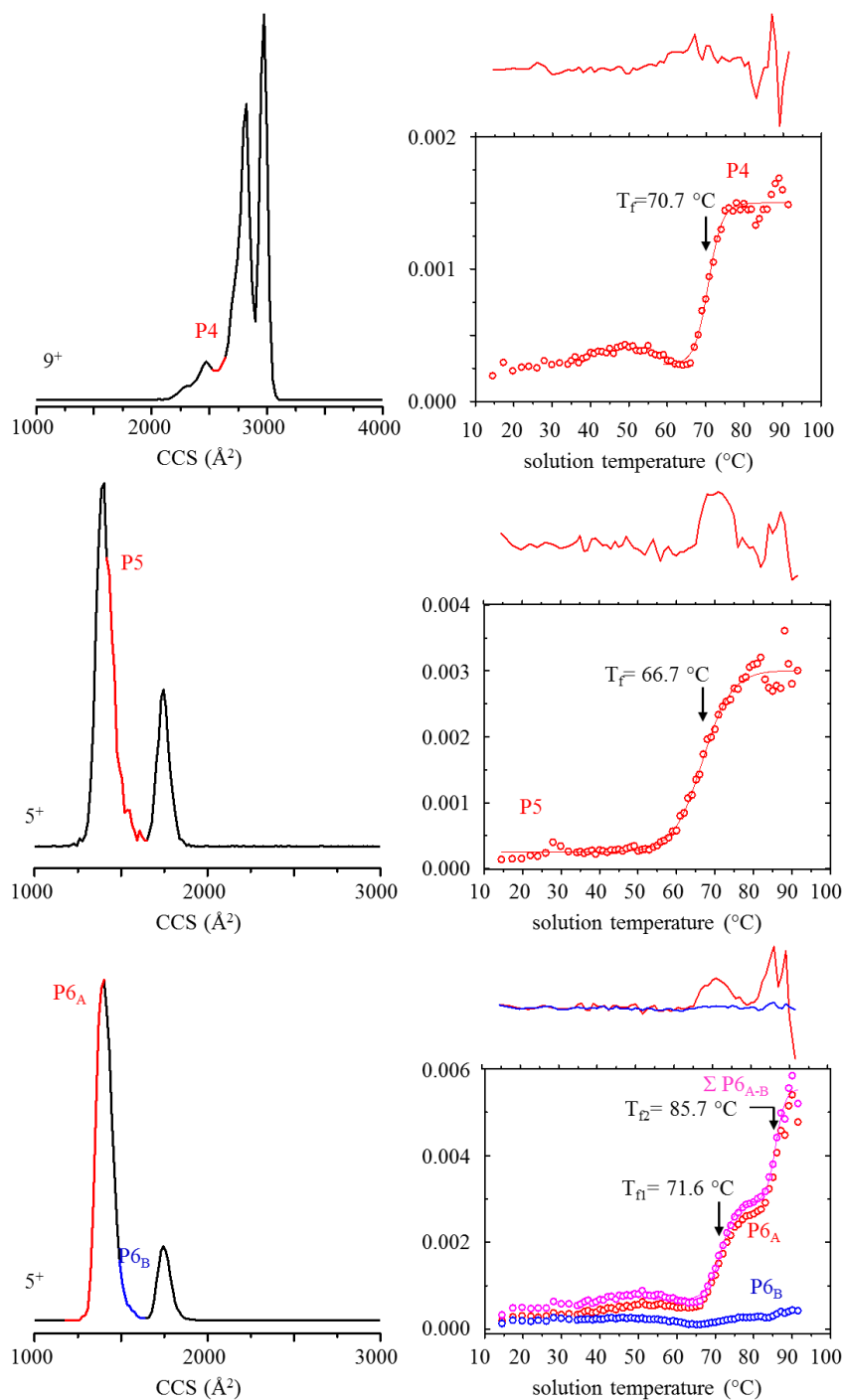
**Figure S6**. CCS distributions of low abundance product conformers P4 – P6 (left), and abundance of these conformers as a function of temperature (right). Colored regions in the CCS traces indicate integral bounds used in abundance plots. First derivative plots used in grouping conformer types are shown in the top right corner of each abundance plot.
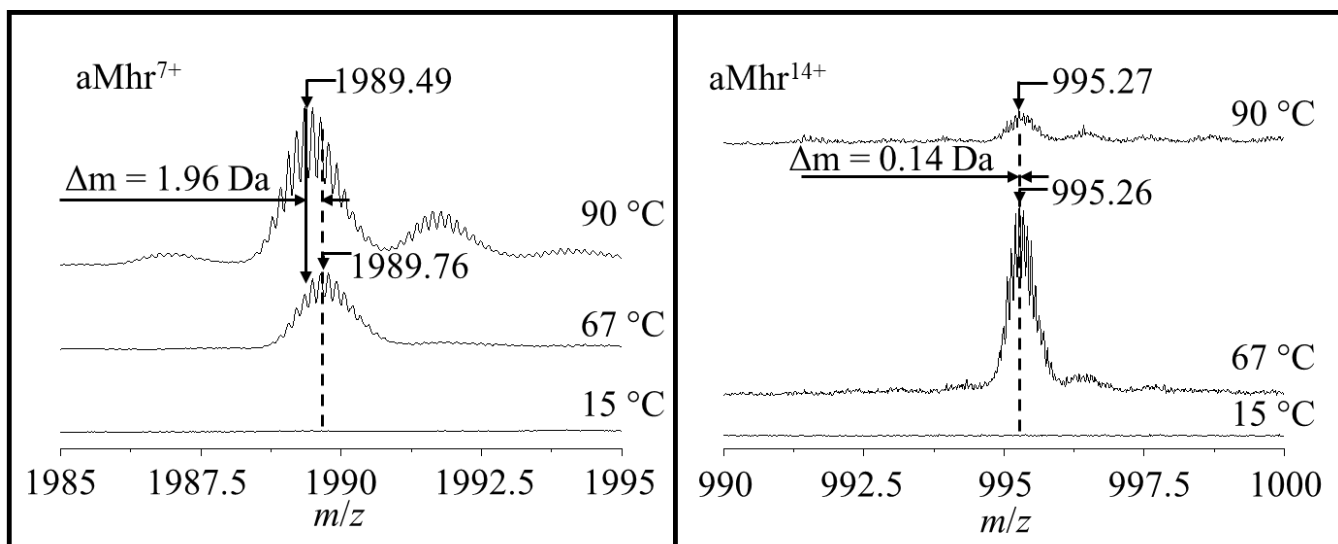
**Figure S7.** Mass spectra of aMhr$^{7+}$ (left) and aMhr$^{14+}$ species (right) at 15, 67, and 90 °C showing change in isotopic peak center at increased temperature as evidence for disulfide formation (theoretical $\Delta m = 2$ Da) in lower charge state aMhr species. A mass shift of 1.96 Da and 0.14 Da is observed for the +7 charge state +14 charge state respectively.
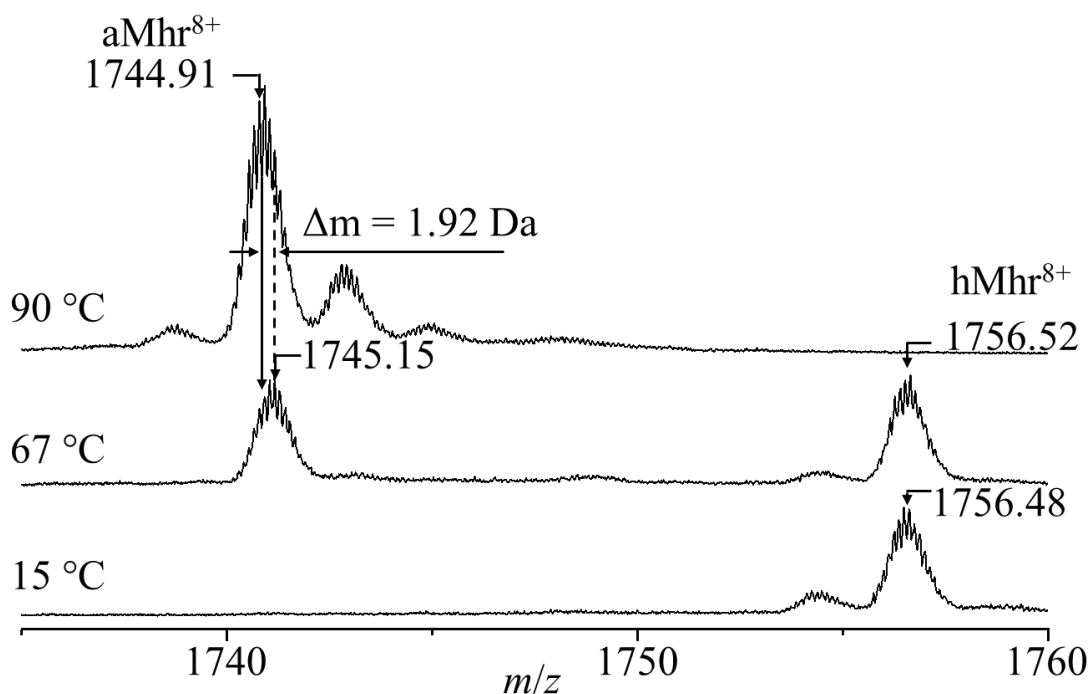
**Figure S8.** Mass spectra of Mhr +8 charge state recorded at 15, 67, and 90 °C showing a decrease in *m/z* in the apo state corresponding to a decrease in mass of ~1.92 Da as evidence for the formation of a disulfide bond in the apo state at high temperatures.

<u>Bottom-up Liquid Chromatography-Mass Spectrometry Sequencing</u>

A 20 µM solution of Mhr in 30 mM ammonium acetate was incubated in a water bath at 90 °C for 1 hr to mimic the conditions of the vT-ESI-IMS-MS experiments. This solution was dried down using a Centrivap concentrator (Labconco, Kansas City, MO), then reconstituted in 100 mM ammonium bicarbonate with 8 M urea. 5 mM iodoacetamide was added to the solution and incubated in the dark for 45 mins. Iodoacetamide was added to alkylate any remaining free cysteine thiols and prevent additional disulfide bond formation during the digestion process. The solution was diluted 8 fold in 100 mM ammonium bicarbonate, and digested with sequencing grade trypsin (Promega, Madison, WI) added at a ratio of 1:100 trypsin:substrate. Peptides were desalted using C18 ZipTips (MilliporeSigma, Burlington, MA), dried down in a Centrivap concentrator, and then resolubilized in buffer A (0.1% formic acid, water, Fisher Scientific, Hampton, NH). Peptides were loaded onto reverse phase trap column (Acclaim

PepMap 100, 75µm × 2 cm, nano viper, C18, 3 µm, 100 Å, ThermoFisher, Waltham, MA) by an easyNanoLC 1200 (ThermoFisher, Waltham, MA) at a flow rate of 5 µL/min for 10 µL. Peptides were resolved using an analytical reverse phase column (Acclaim PepMap RSLC, 75 µm × 25 cm, 2 µm, 100 Å, ThermoFisher, Waltham, MA) over a 24 minute linear gradient from 7% to 40% buffer B (0.1 % formic acid, 80% acetonitrile, 20% $H_2O$, Fisher Scientific, Hanover, NH). Peptides eluting from the analytical column were electrosprayed into a Fusion Lumos Tribrid (Thermo Fisher, Waltham, MA). Precursor ions (scan range: 400-2000 *m/z*) were monitored with a resolving power of 120,000 (@ 200 *m/z*). Precursor ions were selected for tandem mass analysis if they met certain criteria; including: intensity greater than $2.5 \times 10^4$, charge state between z=2 and z=9. Selected precursor ions were quadrupole isolated with an offset from the monoisotopic mass by 0.5 m/z with a window of 2 *m/z*. Peptides were subjected to both higher energy collision dissociation (30 ± 5 %) and supplemental activation electron transfer dissociation (EThcD; calibrated charge dependent ETD parameters, SA HCD energy 20%) and fragment ion masses were measured with a resolving power of 50,000 (@ 200 *m/z*). The AGC target was set to $5.0 \times 10^4$ or a fill time of 86 ms. MS method cycle time was set to 3 sec, and precursor ion dynamic exclusion window was set for 30 seconds (±10 ppm).

Peak lists were generated using Proteome Discoverer 2.1.1.2 (Thermo Fisher, Waltham, MA). Peptide database searching was completed using Protein Prospector against myohemerythrin protein (accession number: P02247). Precursor and fragment ion tolerances were set to 10 ppm and 20 ppm, respectively. Variable modification included acetyl (N-term), acetyl + oxidation (N-term), cysteine carbamidomethyl, cysteine oxidation and dioxidation, glutamine conversion to pyro-glutamic acid (N-term glutamine), methionine loss and methionine loss with acetylation (N-term), and methionine oxidation and dioxidation. Finally, these data were searched using the cross-link functionality, allowing for disulfide bonded peptides.
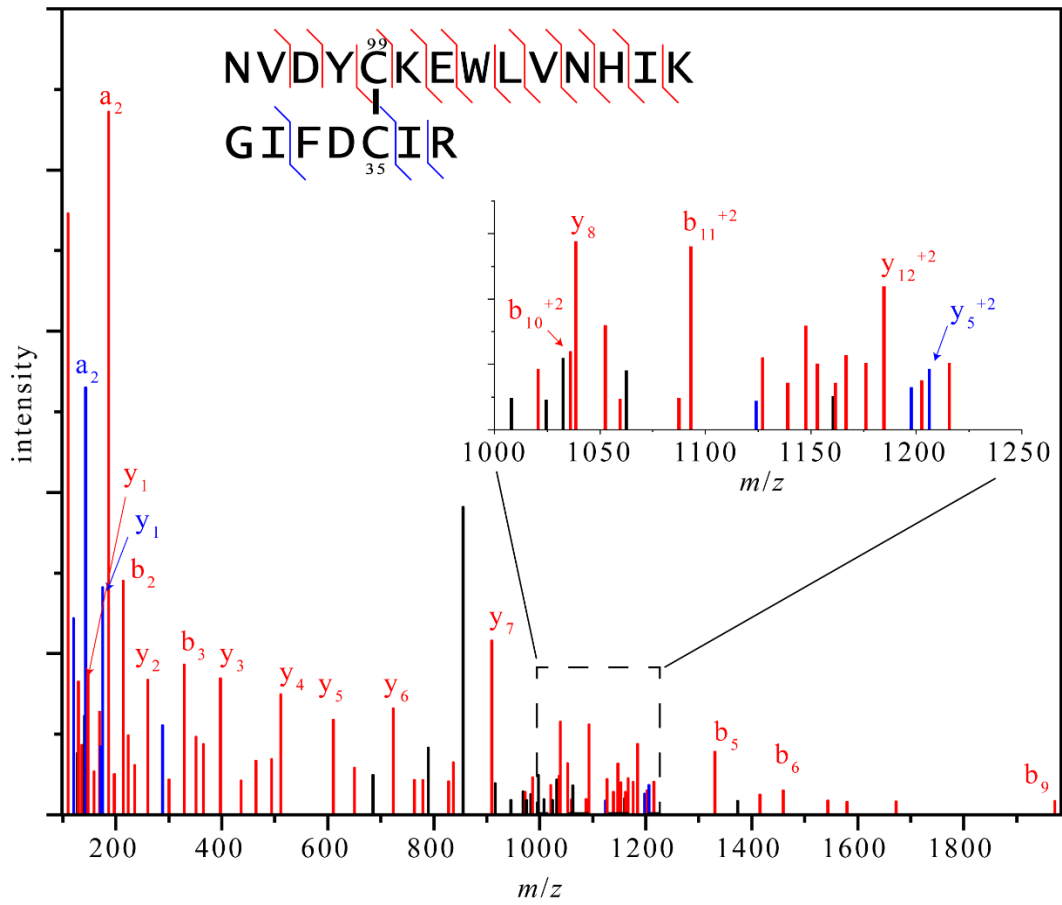
**Figure S9.** HCD MS/MS spectrum showing the positive identification of cross-linked tryptic peptides linked at $Cys_{35}$-$Cys_{95}$ by a disulfide bond.
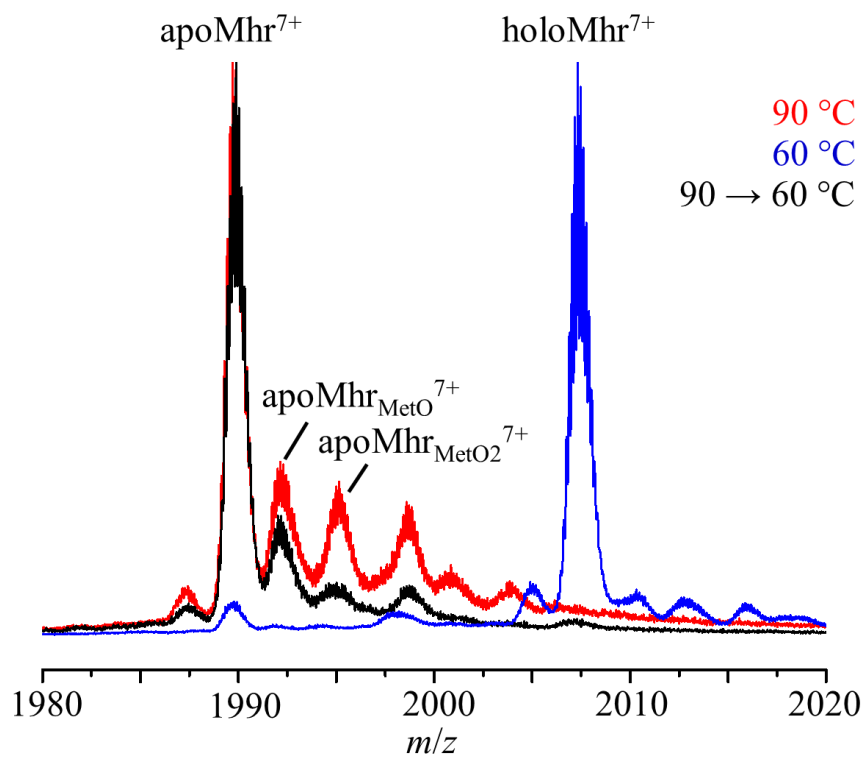
**Figure S10.** Mass spectra of Mhr $7^+$ charge state incubated at high and moderate temperatures. The red trace indicates the sample was incubated at 90 °C, the blue trace at 60 °C. The black trace indicates the sample was incubated at 90 °C, then cooled to 60 °C prior to analysis. All samples were incubated for at least 30 minutes to allow for temperature equilibration.